Reducing the Radar Cross Section of Microstrip Arrays Using AMC Structures for the Vehicle Integration of Automotive Radars

Claudia Vasanelli, *Student Member, IEEE*, Frank Bögelsack, and Christian Waldschmidt, *Senior Member, IEEE*

***Abstract*— Automotive radar sensors for driver assistance systems are usually installed behind the bumper of the car. Multiple reflections between radar and bumper can occur and may lead to a wrong estimation of the direction of arrival of the signal reflected by the target. This paper presents an effective solution to improve the hidden integration of radars in a vehicle. In particular, this paper proposes the design of a low-radar cross section (RCS) millimeter-wave antenna array to reduce the reflections toward the car fascia. The design exploits the properties of artificial magnetic conductors (AMCs) to cancel out the wave backscattered by the antenna array. The integration of the AMC with the antenna array is analyzed in detail. The experimental results prove that the array with low RCS can mitigate the multiple reflections. Moreover, the measurement results show that the proposed antenna has 20 dB RCS reduction at 76 GHz.**

***Index Terms*— Metamaterials, microstrip antenna arrays, millimeter-wave (mm-wave) radar, radar cross section (RCS).**

I. Introduction

RADAR sensors are nowadays commonly employed in the driver assistance systems to measure constantly the surrounding environment helping the driver to control the vehicle and to avoid collisions. The frequency range assigned in many countries to automotive radars is between 76 and 81 GHz. The radar sensors can accurately measure the distance and the velocity of the targets, and they are robust against the harsh weather conditions compared with other sensor technologies [1]. The small wavelength allows to realize compact sensors that can be easily integrated in the vehicle, typically behind the front and rear bumper.

In general, the bumpers are complex multilayer structures composed of low-cost plastic materials. Usually a polypropylene slab is followed by the primer and the coating [2]. The various layers can show significant different values of permittivity, ranging from 2 to 8 [2]. The coating contains in most cases metal particles, which make nontrivial the placement of the radar sensor behind the bumper. Moreover, since the usual thickness of the bumper is in the range of a few millimeters, at millimeter-wave (mm-wave) frequencies the bumper thickness is not electrically thin [3]. The bumper can thus strongly reflect back the wave emitted by the radar sensor.

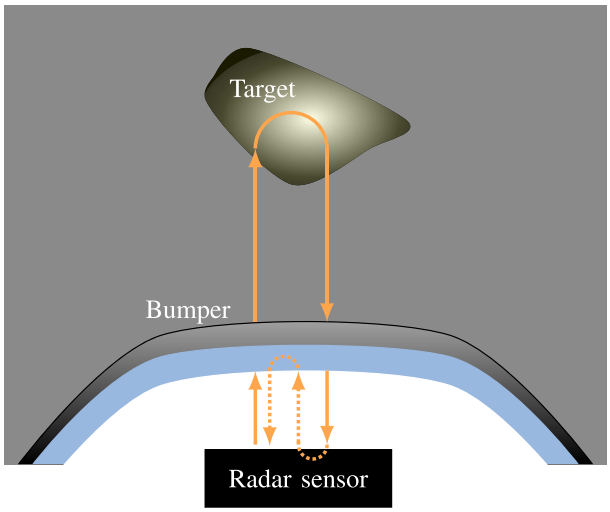

Fig. 1. Multiple reflections between the radar sensor and the bumper of the car. Dotted lines: unwanted contributions due to the backscattering from the radar sensor. A low-RCS radar sensor can mitigate these paths.

As an example, let us consider the scenario shown in Fig. 1. The radar sensor illuminates a target on the street. The wave reflected back by the target will impinge on the metal housing and on the printed circuit board (PCB) of the sensor. The PCB and the metal housing will reflect again the impinging wave toward the bumper, which in turn will reflect again a part of the impinging wave. The antennas of the radar will receive the signal of interest from the target superimposed on the multiple reflections between radar and bumper, and both signals will be detected in the same range cell. Therefore, the problem of multiple reflections can potentially leads to a wrong estimation of the position of the target or angular ambiguities [4], causing for example, a wrong braking intervention.

The angular errors caused by the multiple reflections are particularly critical to radar sensors with a high angular resolution, i.e., with a focused field of view (FoV), which are normally used for the collision avoidance and adaptive cruise control (ACC). On the other hand, radars with a wide FoV, for

Manuscript received June 6, 2017; revised December 18, 2017; accepted December 26, 2017. Date of publication January 17, 2018; date of current version March 1, 2018. *(Corresponding author: Claudia Vasanelli.)*

The authors are with the Institute of Microwave Engineering, University of Ulm, 89081 Ulm, Germany (e-mail: claudia.vasanelli@uni-ulm.de).

Color versions of one or more of the figures in this paper are available online at http://ieeexplore.ieee.org.

Digital Object Identifier 10.1109/TAP.2018.2794410

instance the sensors for blind spot detection, are more robust against angular errors due to their low angular resolution. This paper focuses thus on the former examples of mm-wave radar sensors. The investigation of proper techniques to mitigate the multiple reflections between radar and car fascia is thus of great practical interest, and a possible solution to address this problem is presented in this paper.

Some previous studies already investigated the problem of reducing the reflections from the bumper. For example, Fitzek *et al.* [4] and Pfeiffer and Biebl [5] propose to compensate the reflections of the coating with the inductive strips or frequency selective surfaces (FSSs). In particular, in [4], the proposed solution consists in clamping an FSS layer on the back of the bumper to compensate it. Although this solution has been proven to be effective, it seems too complex in most practical cases. The bumper design must follow indeed specific safety requirements, and it is a crucial element of the aesthetic guidelines of car manufacturers.

Another practical approach to solve the problem of the multiple reflections could be tilting the orientation of the radar sensor with respect to the bumper. Indeed, if the PCB and bumper are not parallel, no multiple reflections are possible, since the wave impinging on the sensor is oblique. This is, however, not an acceptable solution, because the radiation pattern of the sensor might be significantly affected by the tilting, and this can degrade the performance of object detection [2]. Hence, a totally different approach is proposed and analyzed in this paper. In particular, this paper presents, for the first time, a solution independent of the specific bumper design and that can effectively reduce the multiple reflections between sensor and fascia.

Minimizing the reflections between the radar sensor and the bumper means in the end to design a sensor with a low-radar cross section (RCS), since the RCS is the parameter that describes the backscattered power when a target is illuminated by an incident plane wave [6]. Many techniques to reduce the RCS have been proposed, and they are widely employed, in particular, for military applications. However, in the specific case of automotive radar sensors, it is important that the reduction of the RCS is fully compatible with the PCB fabrication process to keep the design of the radar sensor front-end simple and the costs as low as possible.

The design of the low-RCS mm-wave antenna described in this paper is based on a low-RCS surface, which has been deeply investigated, for example, in [7] and [8]. The authors exploit a chessboardlike periodic displacement of two basic elements: an artificial magnetic conductor (AMC) and a perfect electric conductor (PEC). This surface can achieve a significant RCS reduction compared with an equal-size metal plate. More recently, the effectiveness of this solution has been verified at mm-wave frequencies, too [9]. The basic principle of the low-RCS chessboard surface is the mutual phase compensation of the wave reflected by the AMC and the PEC, which permits to achieve destructive interference, and therefore, a reduction of the backscattered wave in a specific direction and at a given frequency. In a similar manner, this design procedure can be retained to develop a novel low-RCS antenna, when the phase of the wave reflected by the AMC is able to compensate the wave reflected by the antenna.

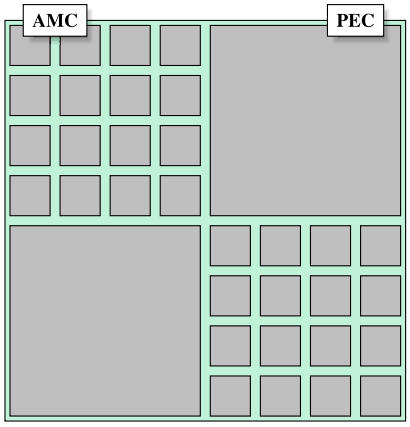

Fig. 2. Unit cell of the chessboardlike low-RCS surface according to [9].

This paper is organized as follows. Section II describes first of all the principle of operation of the low-RCS antenna and explains the effect of the input impedance matching on the backscattering from the array. The details of the design of the proposed antenna are drawn in Section III. Section IV deals with the experimental characterization of the fabricated prototypes, and the main measurement results are discussed. The main outcomes of this paper are summarized in Section V.

II. Principle of Operation

To fully understand the basic principle of the proposed design, it is convenient to briefly describe the chessboardlike low-RCS surface, which is the starting point for the development of the low-RCS antenna. For a full description of the low-RCS surfaces, we suggest to refer to [7]–[9].

The unit cell of the chessboardlike configuration is represented in Fig. 2. The basic building blocks are a periodic displacement of AMC cells and PEC patches. An AMC behaves like a magnetic conductor at the resonance frequency [10], and it can then perfectly compensate the reflection phase of the PEC. That is to say, since the reflection coefficient of an AMC at the resonance frequency is $+1$ and that one of a PEC is -1, destructive interference takes place. The incident wave will not be backscattered in the boresight direction, but redirected in different directions [8]. Unlike other applications of AMC surfaces, such as [11], no absorption of the impinging wave is involved in this case to reduce the RCS of the surface.

The same basic principle can also be applied to the design of a low-RCS antenna. Let us consider a planar antenna, for example a microstrip antenna, and let us surround the array with a set of AMC square patches. In this paper, we will focus only on microstrip antenna arrays, since they are commonly employed in the commercial automotive radars [1], [12]; the design method can also be, however, easily generalized to other planar PCB technologies. If the phase of the wave reflected by the antenna in a specific direction is known, then it is possible to design a proper AMC so that destructive interference can be achieved. More formally, by using the same notation of [8], the approximated amplitude of the

RCS reduction is given by

$$r = 10\log\left|\frac{A_{\mathrm{AMC}}e^{j\varphi_{\mathrm{AMC}}} + A_{\mathrm{ant}}e^{j\varphi_{\mathrm{ant}}}}{2}\right|^2 \ \mathrm{dB}, \qquad (1)$$

where A_{AMC} and A_{ant} are the amplitudes of the reflection coefficients of the AMC and the antenna array, and φ_{AMC} and φ_{ant} are the respective phases. The RCS reduction predicted by (1) is basically an average of the contribution of the antenna array and the AMC. The assumption is that the two components occupy the same area on the PCB. If this is not the case, (1) must be modified into a weighted average, where the weights depend on the area occupation of the AMC and the antenna array.

The prerequisite for the design of the low-RCS antenna array is the knowledge of the backscattering from the antenna array in terms of amplitude and phase. Before going into the details of the design, it is thus necessary to investigate the properties of microstrip arrays as receiving antennas, and in particular the dependence of the backscattered wave on the antenna impedance matching. This is a fundamental point for the proposed design: if the backscattered wave depends on the actual load, then the compensation technique, which we introduce in this paper, to reduce the RCS of the array would be fruitless in all practical cases.

A. Effect of the Load on the Scattering From the Array

The scattering properties are often neglected during the design of antenna arrays. Except for some military or radio frequency identification (RFID) applications, where the RCS signature is of particular interest [13], most of the antenna designers are focused on other important antenna parameters, such as radiation pattern and gain.

As can be intuitively understood, the scattering from an antenna depends on the matching at its input port. A nonideal matching causes indeed a reradiation of the wave traveling toward the feed terminals. More in detail, the RCS of an antenna can be described by two terms: a structural mode and an antenna mode. The structural mode can be measured when the antenna is conjugate matched, and it depends only on the *structural* characteristic of the antenna, such as geometry, materials, and so on. On the other hand, the antenna mode is directly affected by the impedance mismatch due to the nonideal load [13]. Since a more formal description of structural and antenna modes falls outside the purpose of this paper, we suggest the reader to refer to [14] for further details.

By changing the load connected to the input port of an antenna, it is possible to investigate the impact of the matching on the structural mode and the antenna mode. If the antenna is connected to a short circuit the antenna mode can be maximized, while with a conjugate matching it can be minimized. This investigation has been carried out by means of the measurement setup described in Fig. 3. In this setup, the antenna under test (AUT) is connected to a variable attenuator, which is in turn connected to a variable phase shifter with a short circuit at its second port. By changing the settings of attenuator and phase shifter, it is possible to modify the impedance matching, both amplitude and phase,

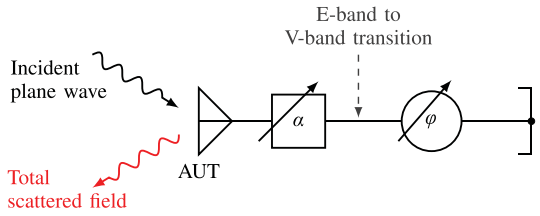

Fig. 3. Measurement setup for the evaluation of the impact of the load on the backscattering of the antenna. The setup is composed of the AUT, a variable attenuator (α), an E- to V-band waveguide transition, a waveguide variable phase shifter (φ), and a short circuit.

Fig. 4. Fabricated series-fed microstrip patch array on RO3003 substrate from Rogers Corporation [19] with 127 μm thickness.

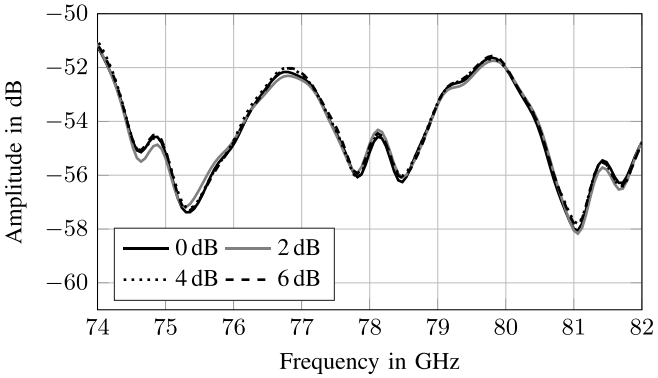

Fig. 5. Measured reflection coefficient by changing the attenuation of the variable attenuator connected to the array.

of the array. The backscattering has been measured with a 25 dBi standard-gain horn antenna placed 2 m apart from the array. The measurement setup is similar to that one described in [9], and for brevity it is here omitted.

The AUT is a 10-element series-fed microstrip patch array designed to operate in the frequency range assigned to automotive radars. The prototype can be seen in Fig. 4. An amplitude tapering is applied to reduce the sidelobe level. The array has been integrated with a microstrip-to-waveguide transition for measurement purposes. As it can be seen, a microstrip probe is inserted inside the rectangular waveguide, which can be then connected perpendicularly to the PCB from the back.

To collect only the signal of interest, time gating has been applied. The measurement results are plotted in Fig. 5. As it can be seen, the amplitude of the measured backscattering is not affected by the change in the impedance matching. Similar results have been obtained by keeping constant the attenuation

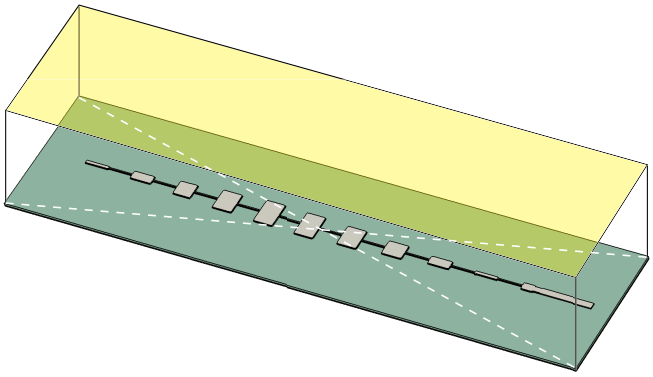

Fig. 6. Model of the series-fed microstrip array used in the 3-D full-wave simulation. The dashed lines highlight the position of the reference plane for the calculation of the reflection coefficient. The yellow area describes the waveguide port to let a plane wave impinge on the array.

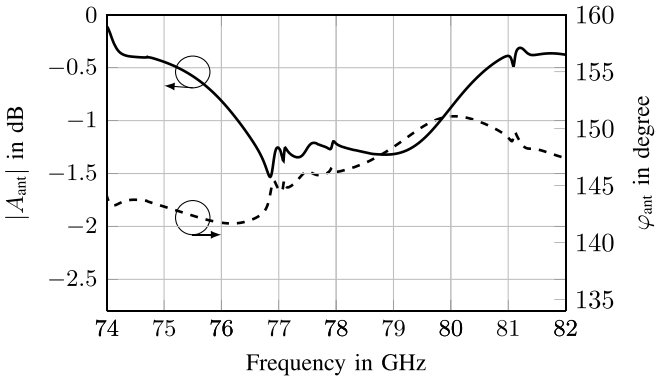

Fig. 7. Full-wave simulation results of the series-fed patch array illuminated by an incident plane wave. Amplitude and phase of the reflection coefficient are depicted in the plot.

at 0 dB from the variable attenuator and changing the phase contribution of the phase shifter only, but they are here omitted for the sake of conciseness. Since, the total scattered field is the superposition of the structural mode and the antenna mode, from this result it can be concluded that the antenna mode is negligible compared with the structural mode for a microstrip patch array. This conclusion is consistent with previous numerical and experimental results presented in the literature only at much lower frequencies, such as [15] and [16].

For designing a mm-wave low-RCS patch array suitable for this application, it is thus sufficient to take into account only the structural mode of the AUT.

III. Design of Low-RCS Antenna Arrays

A. Simulation Setup

The first step toward the design of a microstrip patch array with low RCS is the estimation of the backscattering from the array. If the antenna array is illuminated by an incident plane wave, it is possible to define a reference plane at the antenna position and to calculate finally the amplitude and the phase of the reflection coefficient.

In this paper, the backscattering from the array has been evaluated by means of 3-D full-wave simulations with an electromagnetic field solver software. The model of the antenna is shown in Fig. 6.

A typical way to define a plane wave in full-wave simulations is to set PEC and perfect magnetic conductor walls [17] or to set unit cell boundaries as the boundary conditions. The excitation is then usually fixed by a waveguide port placed above the AUT where a perfectly matched layer is set.

The application of interest, which we investigate in this paper, poses specific challenges with respect to the simulation setup. As explained before, the AUT is a microstrip patch array, whose substrate and ground plane normally extend for many wavelengths in width and height. The waveguide port defined above the AUT has the same dimensions as the array substrate, as can be easily understood from Fig. 6. Hence, due to the large dimensions of the waveguide port, a great number of modes must be taken into account. Moreover, the significant dimensions of the structure set a quite large number of mesh cells to proper discretize the model.

In the simulation setup used in this paper, the unit cell boundary conditions have been employed, since in the simulation software this configuration allows a larger number of higher order modes that can be correctly taken into account. However, the structure that has been investigated is by its nature not periodic. This means, that the coupling between adjacent unit cells must be carefully reduced to avoid simulation artifacts. Moreover, the edges of the array do not contribute to the simulation results since an infinite extent of the structure is assumed.

B. Antenna Structure

With the simulation setup described in Section III-A, the backscattering from a series-fed microstrip patch array has been calculated in terms of amplitude and phase. The same array of Fig. 6 has been used. The metalization of the array has been defined as PEC, and the substrate RO3003 is modeled as lossless to reduce the complexity of the simulation.

The simulation results are plotted in Fig. 7. As it can be seen, the amplitude of the reflection coefficient is less than 0 dB close to the resonance frequency (77 GHz) of the patch antenna array, while the phase is confined between 141° and 151° in the frequency range of interest. In particular, at 77 GHz the reflection phase is 144°. It means that an AMC with a reflection phase of −36° would be able to almost perfectly cancel out the wave backscattered by the antenna array assuming identical amplitudes for the array and the AMC.

To achieve the RCS reduction, a square patch can be used as AMC and integrated on the same substrate of the antenna array. The top view of the unit cell can be seen in Fig. 8.

The dimensions of the square patch have been optimized to compensate the phase of the array at 77 GHz. As can be seen from the simulation results shown in Fig. 9, when the gap between adjacent unit cells is set to 0.13 mm and the edge of the patch has a length of 0.88 mm, it is possible to achieve −33° for the reflection phase at 77 GHz, which is close to the ideal required phase value.

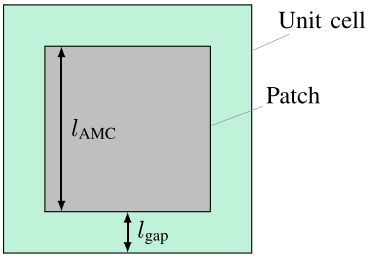

Fig. 8. Top view of the square patch is used as an AMC unit cell. The dimensions are $l_{\text{AMC}} = 0.88$ mm and $l_{\text{gap}} = 0.13$ mm.

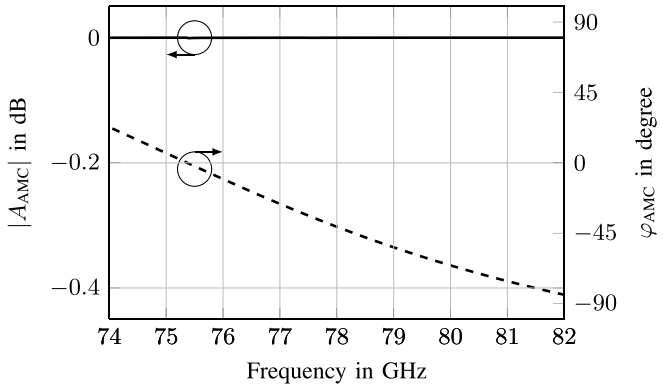

Fig. 9. Full-wave simulation results of the square patch used as AMC illuminated by an incident plane wave. Amplitude and phase of the reflection coefficient are shown in the plot.

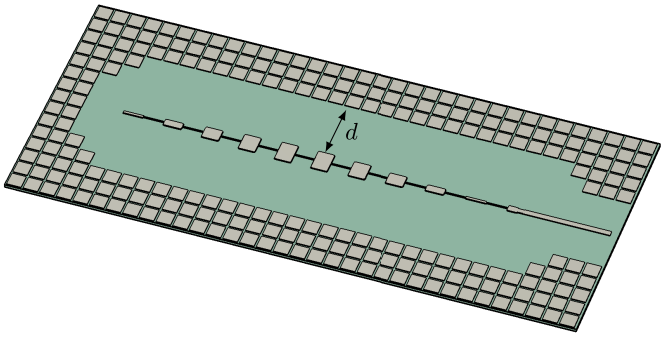

Fig. 10. Model of the series-fed microstrip array integrated with the AMC cells. The distance d between the array and the AMC cells is equal to 3.94 mm (approx. λ_0 at 77 GHz).

The next step is the integration of the AMC with the microstrip array. The placement of the AMC around the array must not affect the main antenna parameters, such as the impedance matching or the radiation pattern. The 3-D model of the integrated structure is shown in Fig. 10.

For example, let the area occupied by the AMC and the antenna array be identical. Then, it is possible to estimate the RCS reduction according to (1). The amplitude is plotted in Fig. 11. As can be seen, the reflection coefficient is significantly reduced around the frequencies where the phase difference between the AMC and the array is 180°. The RCS reduction is better than −10 dB in an almost 5 GHz bandwidth. The use of (1) for the evaluation of the RCS reduction is reasonable under the assumption that there is no strong coupling between the array and the AMC cells. Finally, by changing the area occupied by the square patches of the AMC it is possible to control the RCS reduction.

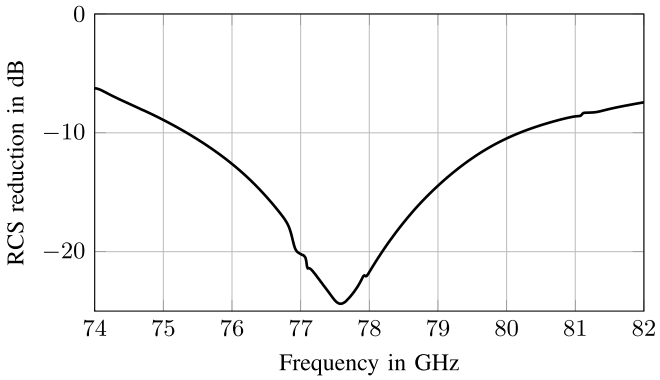

Fig. 11. RCS reduction using (1) after the integration of the AMC around the patch array.

Ideally, the RCS reduction can also be calculated by the means of full-wave simulations. However, due to the limitations of the simulation setup already described in Section III-A, the complexity of the model makes the simulation unfeasible in many practical cases.

C. Limitations of the Design Procedure

As already explained, the full-wave simulation setup used in this paper is not able to take into account large antenna arrays. The prototypes that have been fabricated and tested in this paper and that will be presented in the following parts of this paper, have larger dimensions compared with the simulated one. Moreover, a waveguide-to-microstrip transition has been connected to the feed of the array for measurement purposes, and it has not been taken into account during the evaluation of the backscattering from the array. Thus, a discrepancy between the simulation and measurement results is highly likely.

It is then interesting to understand how significant is a phase or amplitude error for the design of a low-RCS array.

Let us assume, without loss of generality, which the array and the AMC occupy the same amount of area on the PCB and that therefore (1) holds true. From Fig. 12, it can be easily understood that, if the error on the phase of the antenna, namely φ_{ant}, is in the range $\pm 20°$ of the nominal value it is still possible to achieve at least 9 dB RCS reduction.

Similar considerations can be done for errors on the estimated amplitude from the antenna array. Uncertainties on the antenna amplitude up to 5 dB can still lead to at least 7 dB RCS reduction.

In all the practical cases, there will be at the same time errors on the amplitude and the phase of the reflection coefficient. This will of course deteriorate the achievable RCS reduction. However, small errors on the knowledge of the phase or the amplitude can still be tolerated in the design procedure.

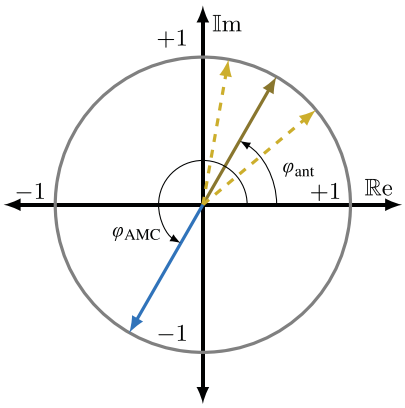

Fig. 12. Effect of a phase error in (1) for the design procedure of the low-RCS antenna shown in a complex coordinate system. The amplitudes of the vectors are assumed equal.

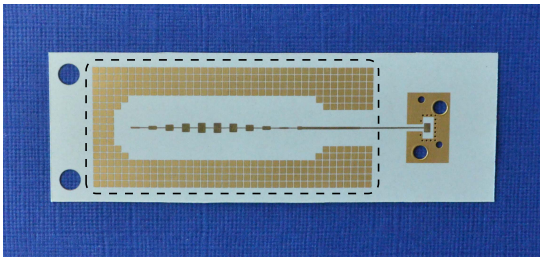

Fig. 13. Fabricated prototype of the low-RCS antenna. The dashed area represents the part of the array illuminated by the horn antenna during the measurement. The outer part of the array has been covered by absorbing material.

IV. Measurement Results

A prototype of a low-RCS antenna array has been fabricated by means of standard photoetching process, and it can be seen in Fig. 13. The visual inspection showed roughly 15 μm etching tolerances. The same substrate as the prototype of Fig. 4 has been used.

In this fabricated model, the area occupied by the AMC corresponds to the 56% of the PCB surface taken into account during the measurements and highlighted by the dashed line in Fig. 13.

A. Effect of the AMC on the Array Performance

First of all, the fabricated prototype has been tested to verify, if the integration of the AMC has any impact on the performance of the patch array in terms of impedance matching and shape of the radiation pattern.

The measured input reflection coefficient can be seen in Fig. 14. The results show that the use of the AMC does not affect significantly the impedance matching of the array in the frequency range of interest. The frequency band, where the amplitude of the reflection coefficient is lower than −10 dB, seems slightly shifted toward higher frequencies for the array with the AMC cells. However, since the two prototypes have been fabricated during different etching processes, it is not possible to draw any conclusion about the impact of the AMC, since this frequency shift is fully compatible also with

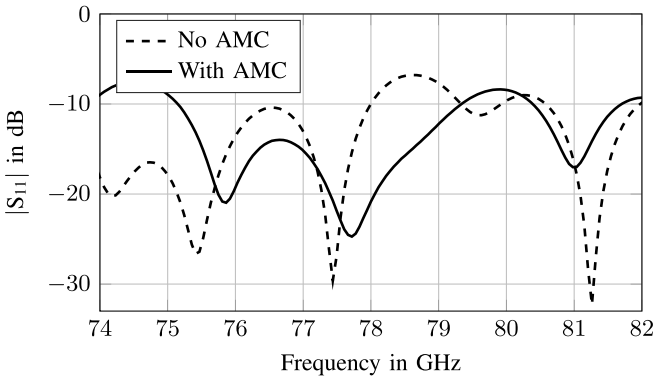

Fig. 14. Measured input reflection coefficient of the arrays with and without the AMC fed by the waveguide-to-microstrip transition.

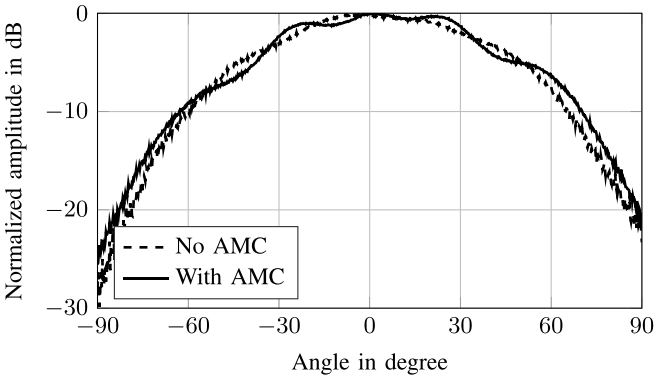

Fig. 15. Measured radiation pattern at 77 GHz in the H-plane.

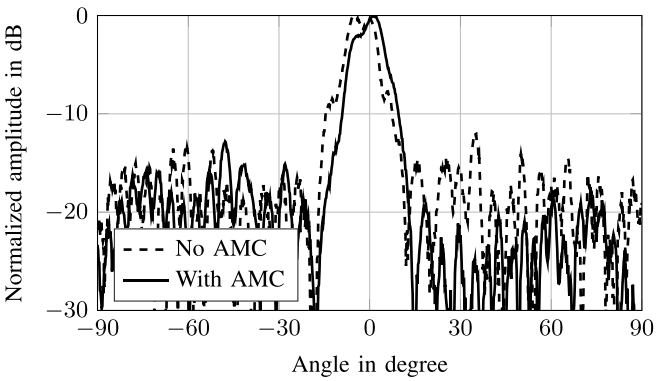

Fig. 16. Measured radiation pattern at 77 GHz in the E-plane.

fabrication inaccuracies or shifts from the nominal value of substrate permittivity, which is likely at mm-wave frequencies.

Figs. 15 and 16 show the radiation pattern at 77 GHz in the H- and E-planes, respectively, measured in an anechoic chamber. The AMC does not affect the shape of the radiation pattern. The sidelobe level and the 3-dB beamwidth of the low-RCS antenna are similar to that one of the standard series-fed patch array. Similar results are obtained at the other frequency points, too.

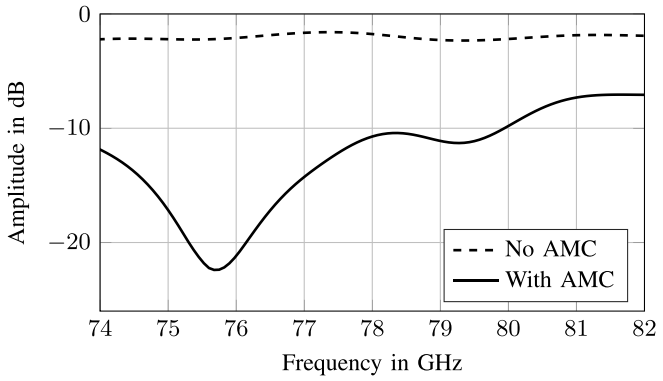

Fig. 17. Measured backscattering from the array with and without AMC for boresight direction. The results are normalized to a measured equal-size metal plate.

B. Characterization of the RCS Reduction

The following step was the evaluation of the RCS reduction. The measurement setup exploits a monostatic configuration similar to that one described in Fig. 3. A standard-gain horn antenna with 25 dBi gain illuminates the AUT, which is placed approximately at a distance of 1.3 m, which satisfies the far-field condition. The AUT is fixed to a plastic mount connected to a stepped motor, which allows controlling accurately its positioning.

To collect only the signal of interest backscattered by the AUT, the time gating has been applied with a 30 GHz frequency span. For a detailed description of the measurement setup settings, we suggest to refer to [9].

To easily evaluate the RCS reduction, the backscattering from a reference metal plate with the same dimensions of the AUT has also been measured.

The measurement results at mm-wave frequencies are sensitive to misalignment and positioning errors. For this reason, a set of 25 measurements has been collected with 3.75 mm steps in horizontal and vertical directions. The final results are then calculated as the average of the 25 different contributions and shown in Fig. 17. In particular, the plot shows the comparison of the backscattered amplitude for the antenna arrays with and without AMC. The integration of the AMC permits to successfully reduce the RCS of the array by approximately 20 dB at 75.7 GHz. Moreover, the RCS reduction is larger than 10 dB in a more than 6 GHz bandwidth.

It is important to verify the properties of the low-RCS antenna in a more realistic scenario, that is to say, behind a typical bumper of a vehicle. In particular, it is interesting to understand what is the impact of using the proposed low-RCS array for instance in the scenario of Fig. 1. However, to evaluate the multiple reflections in such a configuration it is not possible to measure them directly with the AUT, i.e., the radar sensor, since the limited bandwidth does not allow for spatially resolving them. Thus for characterizing the multiple reflections, the measurement setup represented in Fig. 18(a) has been used. As it can be seen, in this monostatic setup, the horn antenna illuminates the AUT, and between them a sample of a standard bumper is placed.

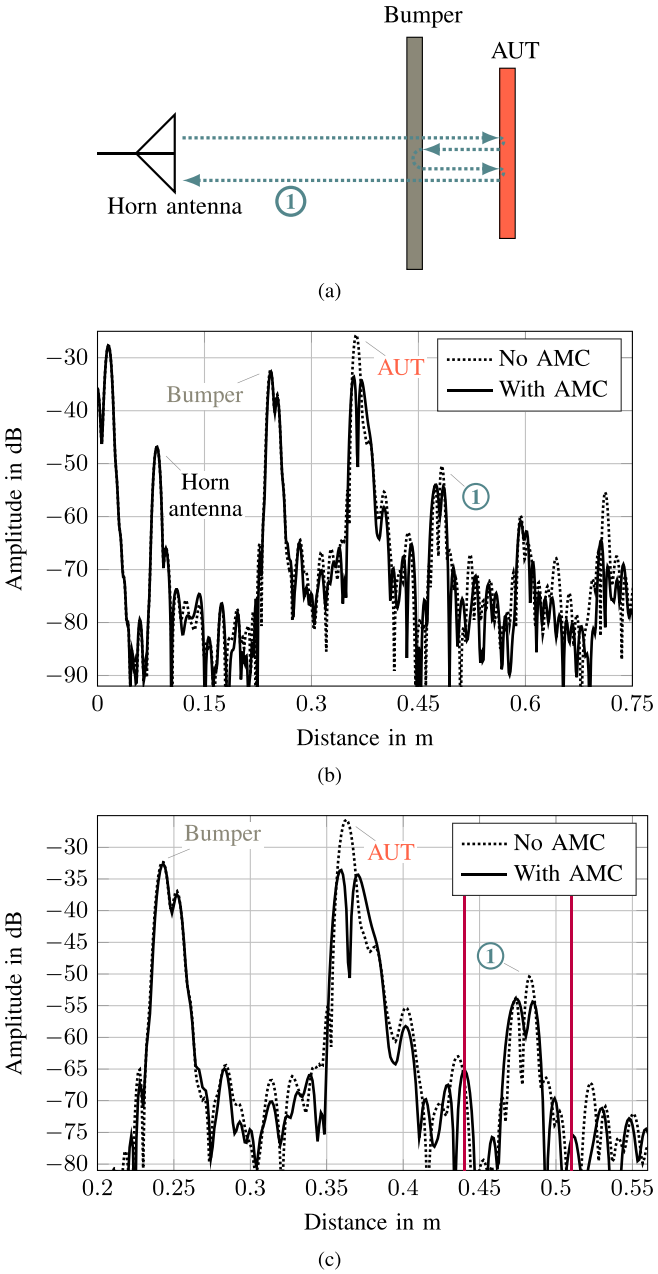

Fig. 18. Testing the low-RCS antenna array behind a sample of a car bumper. In the time domain (b) and (c), it is possible to recognize the multiple reflections. The distance on the abscissa refers to the distance from the reference plane of the one-port calibration, i.e., the rectangular waveguide at the input of the horn antenna. (a) Schematic of the measurement setup. (b) Time domain plot of the measured backscattering. (c) Zoomed-in view of the time domain plot of (b). The purple vertical lines around the position of the first multiple reflection describes the span of the time-gating window that has been used for the results of Fig. 19.

The signal transmitted by the horn antenna basically mimics that signal that would be reflected back by the target in the scenario of Fig. 1. This setup is hence suited for investigating the multiple reflections between the AUT and the bumper. The thickness of the bumper sample is 2.8 mm, and it is metallic silver painted. The distance between the sample and the AUT is 13 cm, which is the minimum distance that can be used in the available measurement setup; this is, however, not a

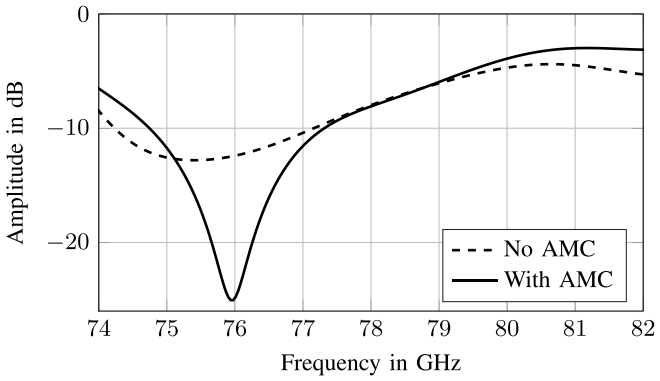

Fig. 19. Plot in the frequency domain of the gated response of the first multiple reflection. The results are normalized to a measured equal-size metal plate.

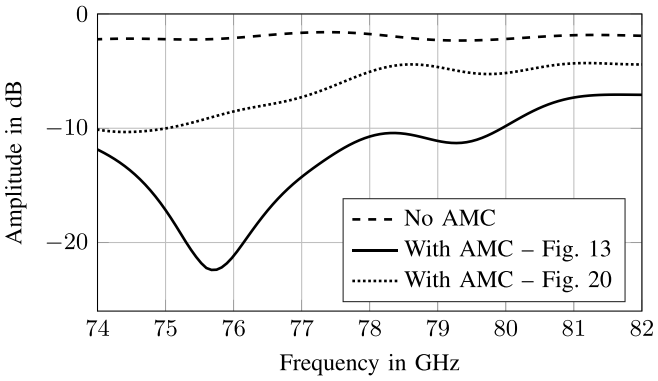

Fig. 21. Comparison of the measured backscattering from the array without AMC and the arrays of Figs. 13 and 20 for incident direction. The results are normalized to a measured equal-size metal plate.

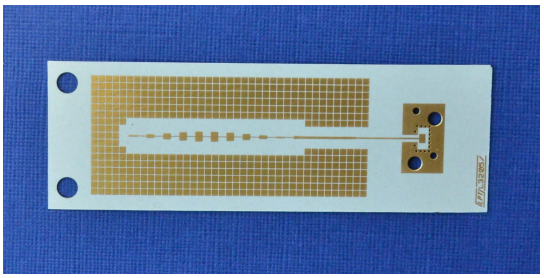

Fig. 20. Fabricated prototype of the low-RCS antenna with an increased area occupied by the AMC.

limitation since in a real scenario the radar sensor is usually mounted a few centimeters away from the bumper [18]. The distance between the horn antenna and the AUT is 28 cm, and thus the measurements have been taken in this case in the near field of the AUT. The reflection coefficient measured by the horn antenna is shown in Fig. 18(b). Fig. 18(c) shows a zoomed-in view of the multiple reflections between the AUT and the bumper sample. Both figures present the measurement results in the time domain to easily and intuitively visualize the problem of the multiple reflections.

As it can be seen in Fig. 18(b) and (c), when the low-RCS array is employed, the amplitude of the backscattered signal is reduced and, consequently, also the amplitude of the multiple reflections. For example, in the measurement results it can be recognized the peak that corresponds to the first multiple reflections at the distance of approximately 0.48 m. With the use of the low-RCS array, the amplitude of this peak can be reduced by 5 dB compared with the case of the standard patch array. In the time domain results there is, however, no explicit information about the frequency content of the signal. To further evaluate the reduction of the first multiple reflection, the time gating has been applied around its peak, using the frequency span highlighted in Fig. 18(c). After filtering out the unwanted part of the signal, the backscattering has been transformed again in the frequency domain and plotted in Fig. 19. As it can be noticed, at 76 GHz the amplitude of the backscattering from the array integrated with the AMC is more than 10 dB smaller than that one from the standard patch array.

C. Varying the Area Occupied by the AMC

To further understand the principle of operation of the low-RCS antenna, it is important to investigate the effect of changing the area occupied by the AMC on the achievable RCS reduction. For this reason, a second prototype has been fabricated and tested, shown in Fig. 20.

In this second version, the area occupied by the AMC cells is significantly larger than in the prototype of Fig. 13. Indeed, in this case 76% of the available surface has been occupied with the AMC.

The measurement results are shown in Fig. 21. As it can be noticed, the increased amount of AMC does not improve the RCS reduction, rather it causes an over-compensation of the backscattering from the antenna array and, hence, the RCS reduction is smaller than in the previous case.

V. Conclusion

In this paper, a mm-wave antenna design to improve the integration of an automotive radar sensor behind the car fascia has been presented. In particular, this paper proposes a novel method to reduce multiple reflections between the radar and the bumper of the car.

The method is based on the integration of a set of square patches acting as an AMC around a planar antenna array. The purpose of the use of an AMC is to achieve a destructive interference between the wave backscattered by the array and by the AMC for a specific direction and in a narrow-band frequency range. The measurement results showed that with this approach it is possible to successfully reduce the RCS of the antenna array by 20 dB at 76 GHz. Moreover, it has been demonstrated that the placement of the AMC around the antenna does not significantly affect the main antenna parameters, such as input impedance and radiation pattern.

The solution proposed in this paper does not increase the complexity and the cost of the fabrication process of the radar sensor front-end, since it is fully compatible with standard PCB photo etching technology, and it is independent of the shape or material composition of the actual bumper.

REFERENCES

[1] J. Hasch, E. Topak, R. Schnabel, T. Zwick, R. Weigel, and C. Waldschmidt, "Millimeter-wave technology for automotive radar sensors in the 77 GHz frequency band," *IEEE Trans. Microw. Theory Techn.*, vol. 60, no. 3, pp. 845–860, Mar. 2012.

[2] R. Schnabel, D. Mittelstrab, T. Binzer, C. Waldschmidt, and R. Weigel, "Reflection, refraction, and self-jamming," *IEEE Microw. Mag.*, vol. 13, no. 3, pp. 107–117, 2012.

[3] J. Dickmann *et al.*, "Making bertha see even more: Radar contribution," *IEEE Access*, vol. 3, pp. 1233–1247, 2015.

[4] F. Fitzek, R. H. Raßhofer, and E. M. Biebl, "Broadband matching of high-permittivity coatings with frequency selective surfaces," in *Proc. German Microw. Conf. (GeMIC)*, Mar. 2011, pp. 1–4.

[5] F. Pfeiffer and E. M. Biebl, "Inductive compensation of high-permittivity coatings on automobile long-range radar radomes," *IEEE Trans. Microw. Theory Techn.*, vol. 57, no. 11, pp. 2627–2632, Nov. 2009.

[6] E. F. Knott, J. F. Shaeffer, and M. T. Tuley, *Radar Cross Section*, 2nd ed. Raleigh, NC, USA: SciTech, 2004.

[7] M. Paquay, J. C. Iriarte, I. Ederra, R. Gonzalo, and P. D. Maagt, "Thin AMC structure for radar cross-section reduction," *IEEE Trans. Antennas Propag.*, vol. 55, no. 12, pp. 3630–3638, Dec. 2007.

[8] W. Chen, C. A. Balanis, and C. R. Birtcher, "Checkerboard EBG surfaces for wideband radar cross section reduction," *IEEE Trans. Antennas Propag.*, vol. 63, no. 6, pp. 2636–2645, Jun. 2015.

[9] C. Vasanelli, F. Boegelsack, and C. Waldschmidt, "Design and experimental characterization of a surface with low radar cross-section at millimeter-wave frequencies," in *Proc. 46th Eur. Microw. Conf. (EuMC)*, London, U.K., 2016, pp. 21–24.

[10] D. Sievenpiper, L. Zhang, R. F. J. Broas, N. G. Alexopolous, and E. Yablonovitch, "High-impedance electromagnetic surfaces with a forbidden frequency band," *IEEE Trans. Microw. Theory Tech.*, vol. 47, no. 11, pp. 2059–2074, Nov. 1999.

[11] F. Costa, A. Monorchio, and G. Manara, "Analysis and design of ultra thin electromagnetic absorbers comprising resistively loaded high impedance surfaces," *IEEE Trans. Antennas Propag.*, vol. 58, no. 5, pp. 1551–1558, May 2010.

[12] W. Menzel and A. Moebius, "Antenna concepts for millimeter-wave automotive radar sensors," *Proc. IEEE*, vol. 100, no. 7, pp. 2372–2379, Jul. 2012.

[13] S. Shrestha, M. D. Balachandran, M. Agarwal, L. H. Zou, and K. Varahramyan, "A method to measure radar cross section parameters of antennas," *IEEE Trans. Antennas Propag.*, vol. 56, no. 11, pp. 3494–3500, Nov. 2008.

[14] J. J. H. Wang, C. Choi, and R. L. Moore, "Precision experimental characterization of the scattering and radiation properties of antennas," *IEEE Trans. Antennas Propag.*, vol. AP-30, no. 1, pp. 108–112, Jan. 1982.

[15] M. A. C. Niamien, S. Collardey, and K. Mahdjoubi, "Absorption and scattering properties of a receiving patch antenna," in *Proc. 9th Eur. Conf. Antennas Propag. (EuCAP)*, Lisbon, Portugal, 2015, pp. 1–4.

[16] S. Hu *et al.*, "Backscattering cross section of ultrawideband antennas," *IEEE Antennas Wireless Propag. Lett.*, vol. 6, pp. 70–73, 2007.

[17] Y. Zhang, J. V. Hagen, M. Younis, C. Fischer, and W. Wiesbeck, "Planar artificial magnetic conductors and patch antennas," *IEEE Trans. Antennas Propag.*, vol. 51, no. 10, pp. 2704–2712, Oct. 2003.

[18] M. Harter, J. Hildebrandt, A. Ziroff, and T. Zwick, "Self-calibration of a 3-D-digital beamforming radar system for automotive applications with installation behind automotive covers," *IEEE Trans. Microw. Theory Techn.*, vol. 64, no. 9, pp. 2994–3000, Sep. 2016.

[19] Rogers Corporation, Rogers, CT, USA.

Claudia Vasanelli (S'12) received the B.Sc. and M.Sc. degrees in telecommunication engineering from the University of Salento, Lecce, Italy. She is currently pursuing the Ph.D. degree with the Institute of Microwave Engineering, University of Ulm, Ulm, Germany.

Since 2014, she has been a Research Assistant with the Institute of Microwave Engineering, University of Ulm. In 2013, she spent one semester as an Exchange Student at the Institute of Radio Frequency Engineering and Electronics, Karlsruhe Institute of Technology, Karlsruhe, Germany. Her current research interests include antenna and array design at mm-wave frequencies, in particular for automotive radar applications.

Mrs. Vasanelli was a recipient of the Young Engineer Prize at the European Microwave Conference in 2016.

Frank Bögelsack received the Dipl.-Ing. degree in electrical engineering from the Braunschweig University of Technology, Braunschweig, Germany, in 1983, and the Dr.-Ing. degree from the University of Duisburg, Duisburg, Germany, in 1989.

He is currently a Senior Researcher and a Lecturer with the Institute of Microwave Engineering, University of Ulm, Ulm, Germany. He is responsible for the antenna and mm-wave measurement facilities.

Christian Waldschmidt (S'01–M'05–SM'13) received the Dipl.-Ing. (M.S.E.E.) and Dr.-Ing. (Ph.D.E.E.) degrees from the Karlsruhe Institute of Technology (KIT), Karlsruhe, Germany, in 2001 and 2004, respectively.

From 2001 to 2004, he was a Research Assistant with the Institut für Höchstfrequenztechnik and Elektronik, KIT. Since 2004, he has been with Robert Bosch GmbH, Stuttgart, Germany, in the business units Corporate Research and Chassis Systems. He was heading different research and development teams in microwave engineering, RF-sensing, and automotive radar. In 2013, he returned to academia. He was appointed as the Director of the Institute of Microwave Engineering at the University of Ulm, Ulm, Germany, where he is currently a Full Professor. He has authored or co-authored over 120 scientific publications and holds over 20 patents. His current research interests include radar and RF-sensing, mm-wave and submillimeter-wave engineering, antennas and antenna arrays, and RF and array signal processing.

Dr. Waldschmidt is the Chair of the IEEE MTT-27 Technical Committee (wireless-enabled automotive and vehicular applications), an Executive Committee Board Member of the German MTT/AP Joint Chapter, and a member of the ITG Committee Microwave Engineering (VDE). In 2015, he served as the TPC Chair and as the TPC Co-Chair for the IEEE Microwave Theory and Techniques Society International Conference on Microwaves for Intelligent Mobility in 2017. He is a Reviewer of multiple IEEE TRANSACTIONS and several conferences, including IMS and EuMW.